A unified treatment of general fluid thermodynamics and its application to a preconditioning scheme

Article *in* Journal of Computational Physics · July 2003

DOI: 10.1016/S0021-9991(03)00211-0

2 authors, including:

Hua Meng
Zhejiang University
48 PUBLICATIONS **1,462** CITATIONS

Available online at www.sciencedirect.com
SCIENCE DIRECT®
Journal of Computational Physics 189 (2003) 277–304
JOURNAL OF COMPUTATIONAL PHYSICS
www.elsevier.com/locate/jcp

A unified treatment of general fluid thermodynamics and its application to a preconditioning scheme

Hua Meng *, Vigor Yang

Department of Mechanical Engineering, The Pennsylvania State University, University Park, PA 16802, USA

Received 28 August 2002; received in revised form 4 December 2002; accepted 27 March 2003

Abstract

A unified treatment of general fluid thermodynamics is developed to handle fluid flows over their entire thermodynamic states. The analysis is based on the concepts of partial-mass and partial-density properties, and accommodates thermodynamic non-idealities and transport anomalies in the transcritical regime. The resultant routine is incorporated into a preconditioning scheme. All the thermophysical properties and numerical Jacobian matrices are derived directly from fundamental thermodynamic theories, rendering a robust algorithm valid for fluid flows at all speeds and at all thermodynamic states. As a specific example, a modified Soave–Redlich–Kwong equation of state is employed to obtain the fluid p–V–T properties. Several test cases concerning supercritical droplet vaporization in both quiescent and convective environments are presented to demonstrate the effectiveness of the present algorithm.

AMS: 65M05; 80A15

Keywords: General fluid thermodynamics; Supercritical droplet vaporization; All-speed fluid flows; Preconditioning method

1. Introduction

Many fluid mechanical devices involve thermodynamic phase transition from a subcritical to a supercritical state. A notable example is high-pressure combustion chambers (such as diesel, gas-turbine, and rocket engines) operating at pressures and temperatures well above the thermodynamic critical points of the injected fuels. The fluids, initially delivered to the chamber at a subcritical temperature, heat up rapidly due to the energy transfer from the ambience and eventually reach their supercritical conditions. The process inherently includes an array of intricate phenomena, especially during the transition through the transcritical regime, where thermodynamic non-idealities and transport anomalies occur [1]. There currently exists,

* Corresponding author.
E-mail address: hxm14@psu.edu (H. Meng).

0021-9991/03/$ - see front matter
doi:10.1016/S0021-9991(03)00211-0

however, no efficient numerical algorithm capable of treating fluid flows over their entire thermodynamic regimes from condensed-liquid to dilute-gas states, although a solid foundation has been established in connection with the study of supercritical droplet vaporization [2–4], spray field dynamics [5,6], and cryogenic propellant combustion [7]. The major obstacles lie in the difficulties in treating thermodynamic and transport properties in a manner consistent with the intrinsic characteristics of a numerical algorithm. The rapid variation of fluid state poses another serious challenge.

The purpose of this paper is to develop a unified numerical treatment of general fluid thermodynamics valid for the entire range of fluid states. The concepts of partial-mass and partial-density properties are employed in fluid mixtures. Fundamental thermodynamic theories are implemented to derive all thermodynamic properties and numerical relations. Furthermore, full account is taken of transport property variations as functions of fluid density, temperature, and composition. The resultant property evaluation routine and numerical Jacobian matrices are incorporated into a preconditioning scheme, rendering an algorithm capable of solving fluid flows at all speeds and at all thermodynamic states. As a specific example, a modified Soave–Redlich–Kwong (SRK) equation of state is used to obtain the thermophysical and numerical properties required in developing a preconditioning code. Several test cases on supercritical droplet vaporization in both quiescent and convective environments are presented to demonstrate the robustness and efficiency of the present algorithm.

2. Theoretical formulation

2.1. Conservation equations

The conservation equations of mass, momentum, energy, and species concentration for a two-dimensional multicomponent chemically reacting system of N species can be expressed as

$$\frac{\partial Q}{\partial t}+\frac{\partial(E-E_v)}{\partial x}+\frac{\partial(F-F_v)}{\partial y}=S, \tag{2.1}$$

where the dependent variable Q is defined as

$$Q=y^{\delta}[\,\rho \quad \rho u \quad \rho v \quad \rho e_t \quad \rho Y_i\,]^{\mathrm{T}}. \tag{2.2}$$

The exponent $\delta=0$ and 1 correspond to a planar two-dimensional and an axisymmetric case, respectively. Standard notation in fluid mechanics is used here, with ρ, (u,v), e_t, and Y_i denoting the density, velocity components, specific total energy, and mass fraction of species i, respectively.

Two fundamental issues have been identified to cause the difficulty in achieving convergence using a time-marching scheme when dealing with low-speed flows: machine round-off errors associated with the calculation of the pressure gradient in the momentum equation, and numerical stiffness arising from eigenvalue disparity. While the latter will be circumvented by introducing a preconditioning term in Section 5.1, the former can be easily overcome by decomposing the pressure into a constant and a fluctuating part as follows [8,9]:

$$p=p_0+p_{\mathrm{g}}. \tag{2.3}$$

The constant pressure p_0 should be taken so as to comprise the majority of p. The gauge pressure p_{g} amounts to the dynamic pressure responsible for the momentum balance that drives the flow. With this representation of pressure, and noting that $\nabla(p_0+p_{\mathrm{g}})=\nabla p_{\mathrm{g}}$, the convective and diffusion flux vectors in Eq. (2.1) take the form of:

$$E = y^{\delta}\begin{bmatrix} \rho u \\ \rho u^2 + p_g \\ \rho uv \\ (\rho e_t + p)u \\ \rho u Y_i \end{bmatrix}, \tag{2.4}$$

$$F = y^{\delta}\begin{bmatrix} \rho v \\ \rho uv \\ \rho v^2 + p_g \\ (\rho e_t + p)v \\ \rho v Y_i \end{bmatrix}, \tag{2.5}$$

$$E_v = y^{\delta}\begin{bmatrix} 0 \\ \tau_{xx} \\ \tau_{xy} \\ u\tau_{xx} + v\tau_{xy} - q_x \\ -\rho \hat{u}_i Y_i \end{bmatrix}, \tag{2.6}$$

$$F_v = y^{\delta}\begin{bmatrix} 0 \\ \tau_{xy} \\ \tau_{yy} \\ u\tau_{xy} + v\tau_{yy} - q_y \\ -\rho \hat{v}_i Y_i \end{bmatrix}, \tag{2.7}$$

where $\hat{u}_i$ and $\hat{v}_i$ are the diffusion velocities of species i in the x- and y-directions, respectively. In the above equations, the normal and shear stresses are given as:

$$\tau_{xx} = \mu\left(\frac{4}{3}\frac{\partial u}{\partial x} - \frac{2}{3}\frac{\partial v}{\partial y}\right), \tag{2.8a}$$

$$\tau_{yy} = \mu\left(\frac{4}{3}\frac{\partial v}{\partial y} - \frac{2}{3}\frac{\partial u}{\partial x}\right), \tag{2.8b}$$

$$\tau_{xy} = \mu\left(\frac{\partial v}{\partial x} + \frac{\partial u}{\partial y}\right), \tag{2.8c}$$

where μ represents the viscosity. The thermal diffusion terms contain contributions from heat conduction and mass diffusion

$$q_x = -k\frac{\partial T}{\partial x} + \rho\sum_{i=1}^{N}\bar{h}_i Y_i \hat{u}_i, \quad q_y = -k\frac{\partial T}{\partial y} + \rho\sum_{i=1}^{N}\bar{h}_i Y_i \hat{v}_i, \tag{2.9}$$

where T is the temperature, k the thermal conductivity, and $\bar{h}_i$ is the partial-mass enthalpy of species i defined in Section 2.2. Fick's law is used to approximate species diffusion in a multicomponent mixture

$$Y_i\hat{u}_i = -D_{i\mathrm{m}}\frac{\partial Y_i}{\partial x}, \quad Y_i\hat{v}_i = -D_{i\mathrm{m}}\frac{\partial Y_i}{\partial y}, \tag{2.10}$$

where $D_{i\mathrm{m}}$ is the effective mass diffusion coefficient of species i.

The source term in Eq. (2.1), S, arises from chemical reactions and axisymmetric geometry

$$S = \begin{bmatrix} 0 \\ \delta\left[-\frac{\partial}{\partial x}\left(\frac{2}{3}\mu v\right)\right] \\ \delta\left[p_g - \frac{4}{3}\frac{\mu v}{y} + \frac{2}{3}\mu\frac{\partial u}{\partial x} - \frac{2}{3}v\frac{\partial \mu}{\partial y}\right] \\ \delta\left[-\frac{\partial}{\partial x}\left(\frac{2}{3}\mu u v\right) - \frac{\partial}{\partial y}\left(\frac{2}{3}\mu v^2\right)\right] \\ y^{\delta}\dot{\omega}_i \end{bmatrix}, \tag{2.11}$$

where $\dot{\omega}_i$ is the rate of change of species i due to chemical reactions.

2.2. Partial-mass and partial-density properties

For a general fluid mixture at a specified state, each constituent component will experience the same temperature, but different partial pressure, and its properties, such as the specific enthalpy in Eq. (2.9), should be defined based on the concept of partial properties. According to classical thermodynamic theories, any extensive thermodynamic property of a mixture at equilibrium, $m\phi$, can be expressed as a function of temperature, T, pressure, p, and partial masses of all components, m_i,

$$m\phi = m\phi(T, p, m_i), \tag{2.12}$$

where m is the total mass of the mixture and ϕ is the specific property per unit mass of a fluid mixture. Eq. (2.12) leads to the definition of partial-mass property

$$\bar{\phi}_i = \left(\frac{\partial m\phi}{\partial m_i}\right)_{T,p,m_{j\neq i}}, \tag{2.13}$$

where the indices, i and j, range from 1 to N. The partial mass enthalpy of species i can thus be expressed as

$$\bar{h}_i = \left(\frac{\partial mh}{\partial m_i}\right)_{T,p,m_{j\neq i}}. \tag{2.14}$$

To facilitate numerical treatment, we also need to define partial-density properties using the following thermodynamic relation:

$$\rho\phi = \rho\phi(T, \rho_i), \tag{2.15}$$

where ρ_i is the density of species i. The partial-density property, $\tilde{\phi}_i$, thus can be defined as

$$\tilde{\phi}_i = \left(\frac{\partial \rho\phi}{\partial \rho_i}\right)_{T,\rho_{j\neq i}}. \tag{2.16}$$

The partial-density enthalpy of species i becomes

$$\tilde{h}_i = \left(\frac{\partial \rho h}{\partial \rho_i}\right)_{T,\rho_{j\neq i}}. \tag{2.17}$$

A general relationship exists between the partial-density and the partial-mass properties

$$\tilde{\phi}_i = \bar{\phi}_i + \rho\left(\frac{\partial \phi}{\partial p}\right)_{T,Y_j}\left(\frac{\partial p}{\partial \rho_i}\right)_{T,\rho_{j\neq i}}. \tag{2.18}$$

We start the proof of the above equation with the differential expression of Eq. (2.12) and the application of Eq. (2.13)

$$\mathrm{d}m\phi = \left(\frac{\partial m\phi}{\partial T}\right)_{p,m_i} \mathrm{d}T + \left(\frac{\partial m\phi}{\partial p}\right)_{T,m_i} \mathrm{d}p + \sum_{i=1}^{N} \bar{\phi}_i \,\mathrm{d}m_i. \tag{2.19}$$

By dividing Eq. (2.19) by the volume, V, and employing the well-known Euler equation in thermodynamics [10]

$$m\phi = \sum_{i=1}^{N} m_i \bar{\phi}_i, \tag{2.20}$$

we obtain the following formula:

$$\mathrm{d}\rho\phi = \frac{1}{V}\left(\frac{\partial m\phi}{\partial T}\right)_{p,m_i} \mathrm{d}T + \frac{1}{V}\left(\frac{\partial m\phi}{\partial p}\right)_{T,m_i} \mathrm{d}p + \sum_{i=1}^{N} \bar{\phi}_i \,\mathrm{d}\rho_i. \tag{2.21}$$

Because mass is conserved for a given system, it can be removed from the differential operation. The above equation can be simplified as follows:

$$\mathrm{d}\rho\phi = \rho\left(\frac{\partial \phi}{\partial T}\right)_{p,Y_i} \mathrm{d}T + \rho\left(\frac{\partial \phi}{\partial p}\right)_{T,Y_i} \mathrm{d}p + \sum_{i=1}^{N} \bar{\phi}_i \,\mathrm{d}\rho_i. \tag{2.22}$$

The differential form of an equation of state, $p = p(T, \rho_i)$, is written as

$$\mathrm{d}p = \left(\frac{\partial p}{\partial T}\right)_{\rho_i} \mathrm{d}T + \sum_{i=1}^{N} \left(\frac{\partial p}{\partial \rho_i}\right)_{T,\rho_{j\neq i}} \mathrm{d}\rho_i. \tag{2.23}$$

Substitution of Eq. (2.23) into Eq. (2.22) leads to the following relationship:

$$\mathrm{d}\rho\phi = \rho\left(\frac{\partial \phi}{\partial T}\right)_{p,Y_i} \mathrm{d}T + \sum_{i=1}^{N} \left(\rho\left(\frac{\partial \phi}{\partial p}\right)_{T,Y_i}\left(\frac{\partial p}{\partial \rho_i}\right)_{T,\rho_{j\neq i}} + \bar{\phi}_i\right) \mathrm{d}\rho_i. \tag{2.24}$$

Eq. (2.18) is thus established by comparing Eq. (2.24) with the differential form of Eq. (2.15) written below:

$$\mathrm{d}\rho\phi = \left(\frac{\partial \rho\phi}{\partial T}\right)_{\rho_i} \mathrm{d}T + \sum_{i=1}^{N} \tilde{\phi}_i \,\mathrm{d}\rho_i. \tag{2.25}$$

3. Thermodynamic relationships for general fluid mixtures

In developing a numerical algorithm for general fluid mixtures, several new relationships based on fundamental thermodynamic theories are required for deriving numerical properties such as Jacobian matrices and system eigenvalues.

3.1. Enthalpy as function of pressure, density, and mass fraction

For a general fluid mixture consisting of N species, every intensive thermodynamic property can be expressed as a function of the other $N + 1$ independent intensive variables. This leads to the following relationship:

$$\rho e = \rho e(T, \rho_i), \quad \text{where } i = 1, 2, \ldots, N, \tag{3.1}$$

where e is the internal energy per unit mass. The differential form of Eq. (3.1) is

$$\mathrm{d}\rho e = \rho\left(\frac{\partial e}{\partial T}\right)_{\rho_i} \mathrm{d}T + \sum_{i=1}^{N}\left(\frac{\partial \rho e}{\partial \rho_i}\right)_{T,\rho_{j\neq i}} \mathrm{d}\rho_i. \tag{3.2}$$

The derivative in the first term on the right-hand side is the constant-volume heat capacity, C_v, and the derivative in the second term is the partial-density internal energy, $\tilde{e}_i$,

$$\tilde{e}_i = \left(\frac{\partial \rho e}{\partial \rho_i}\right)_{T,\rho_{j\neq i}}. \tag{3.3}$$

Eq. (3.2) now takes the form

$$\mathrm{d}\rho e = \rho C_v \mathrm{d}T + \sum_{i=1}^{N} \tilde{e}_i \mathrm{d}\rho_i. \tag{3.4}$$

We may change the summation on the right-hand side of Eq. (2.23) from 1 through N to 1 through $N-1$ to obtain the following relation:

$$\mathrm{d}T = \left\{ \mathrm{d}p - \sum_{i=1}^{N-1}\left[\left(\frac{\partial p}{\partial \rho_i}\right)_{T,\rho_{j\neq i}} - \left(\frac{\partial p}{\partial \rho_N}\right)_{T,\rho_{j\neq N}}\right]\mathrm{d}\rho_i - \left(\frac{\partial p}{\partial \rho_N}\right)_{T,\rho_{j\neq N}} \mathrm{d}\rho \right\} \Bigg/ \left(\frac{\partial p}{\partial T}\right)_{\rho_i}. \tag{3.5}$$

Substitution of Eq. (3.5) into Eq. (3.4) leads to

$$\begin{aligned}\mathrm{d}\rho e = {} & \rho C_v\left(\frac{\partial T}{\partial p}\right)_{\rho_i} \mathrm{d}p + \sum_{i=1}^{N} \tilde{e}_i \mathrm{d}\rho_i - \rho C_v\left(\frac{\partial T}{\partial p}\right)_{\rho_i}\left(\frac{\partial p}{\partial \rho_N}\right)_{T,\rho_{j\neq N}} \mathrm{d}\rho \\ & - \rho C_v\left(\frac{\partial T}{\partial p}\right)_{\rho_i} \sum_{i=1}^{N-1}\left[\left(\frac{\partial p}{\partial \rho_i}\right)_{T,\rho_{j\neq i}} - \left(\frac{\partial p}{\partial \rho_N}\right)_{T,\rho_{j\neq N}}\right]\mathrm{d}\rho_i.\end{aligned} \tag{3.6}$$

The term on the left-hand side can be rewritten as

$$\mathrm{d}\rho e = \rho\,\mathrm{d}e + e\,\mathrm{d}\rho. \tag{3.7}$$

Substitution of Eq. (3.7) into Eq. (3.6) yields

$$\begin{aligned}\mathrm{d}e = {} & C_v\left(\frac{\partial T}{\partial p}\right)_{\rho_i} \mathrm{d}p - C_v\left(\frac{\partial T}{\partial p}\right)_{\rho_i}\left(\frac{\partial p}{\partial \rho_N}\right)_{T,\rho_{j\neq N}} \mathrm{d}\rho - C_v\left(\frac{\partial T}{\partial p}\right)_{\rho_i} \sum_{i=1}^{N-1}\left[\left(\frac{\partial p}{\partial \rho_i}\right)_{T,\rho_{j\neq i}} - \left(\frac{\partial p}{\partial \rho_N}\right)_{T,\rho_{j\neq N}}\right]\mathrm{d}\rho_i \\ & + \frac{1}{\rho}\sum_{i=1}^{N-1}(\tilde{e}_i - \tilde{e}_N)\,\mathrm{d}\rho_i + \frac{\tilde{e}_N}{\rho}\,\mathrm{d}\rho - \frac{e}{\rho}\,\mathrm{d}\rho.\end{aligned} \tag{3.8}$$

The enthalpy can be related to the internal energy through its definition

$$\mathrm{d}h = \mathrm{d}e + \frac{1}{\rho}\,\mathrm{d}p - \frac{p}{\rho^2}\,\mathrm{d}\rho. \tag{3.9}$$

Substitution of Eq. (3.8) into Eq. (3.9) establishes an explicit expression for enthalpy

$$\mathrm{d}h = \left[C_v\left(\frac{\partial T}{\partial p}\right)_{\rho_i} + \frac{1}{\rho}\right]\mathrm{d}p + \left[-C_v\left(\frac{\partial T}{\partial p}\right)_{\rho_i}\left(\frac{\partial p}{\partial \rho}\right)_{T,Y_i} + \frac{1}{\rho}\sum_{i=1}^{N} Y_i\tilde{e}_i - \frac{e}{\rho} - \frac{p}{\rho^2}\right]\mathrm{d}\rho + \sum_{i=1}^{N-1}\left\{-\rho C_v\left(\frac{\partial T}{\partial p}\right)_{\rho_i}\left[\left(\frac{\partial p}{\partial \rho_i}\right)_{T,\rho_{j\neq i}} - \left(\frac{\partial p}{\partial \rho_N}\right)_{T,\rho_{j\neq N}}\right] + (\tilde{e}_i - \tilde{e}_N)\right\}\mathrm{d}Y_i. \tag{3.10a}$$

Since Eq. (3.10a) will be frequently applied for deriving numerical Jacobians, we introduce the following definitions for convenience:

$$A_p = C_v\left(\frac{\partial T}{\partial p}\right)_{\rho_i} + \frac{1}{\rho}, \tag{3.10b}$$

$$A_\rho = -C_v\left(\frac{\partial T}{\partial p}\right)_{\rho_i}\left(\frac{\partial p}{\partial \rho}\right)_{T,Y_i} + \frac{1}{\rho}\sum_{i=1}^{N} Y_i\tilde{e}_i - \frac{e}{\rho} - \frac{p}{\rho^2}, \tag{3.10c}$$

$$A_{Y_i} = -\rho C_v\left(\frac{\partial T}{\partial p}\right)_{\rho_i}\left[\left(\frac{\partial p}{\partial \rho_i}\right)_{T,\rho_{j\neq i}} - \left(\frac{\partial p}{\partial \rho_N}\right)_{T,\rho_{j\neq N}}\right] + (\tilde{e}_i. - \tilde{e}_N). \tag{3.10d}$$

A thermodynamic relationship defining enthalpy as a function of pressure, density, and mass fractions can then be expressed as

$$\mathrm{d}h = A_p\,\mathrm{d}p + A_\rho\,\mathrm{d}\rho + \sum_{i=1}^{N-1} A_{Y_i}\,\mathrm{d}Y_i. \tag{3.10e}$$

3.2. Enthalpy as function of pressure, temperature, and mass fraction

In this section, a thermodynamic relationship defining enthalpy as a function of pressure, temperature, and mass fraction will be developed. We start with the following relationship:

$$\mathrm{d}\rho_i = \rho\,\mathrm{d}Y_i + Y_i\,\mathrm{d}\rho. \tag{3.11}$$

Substitution of Eq. (3.11) into Eq. (3.4) leads to

$$\mathrm{d}\rho e = \rho C_v\,\mathrm{d}T + \sum_{i=1}^{N}\rho\tilde{e}_i\,\mathrm{d}Y_i + \sum_{i=1}^{N} Y_i\tilde{e}_i\,\mathrm{d}\rho. \tag{3.12}$$

Substitution of Eq. (3.7) into Eq. (3.12) yields

$$\mathrm{d}e = C_v\,\mathrm{d}T + \sum_{i=1}^{N-1}\left(\tilde{e}_i - \tilde{e}_N\right)\mathrm{d}Y_i + \frac{1}{\rho}\left(\sum_{i=1}^{N} Y_i\tilde{e}_i - e\right)\mathrm{d}\rho. \tag{3.13}$$

Incorporation of Eq. (3.11) into Eq. (3.5) results in a thermodynamic relationship for density as a function of temperature, pressure, and mass fraction

$$\mathrm{d}\rho = \left\{\mathrm{d}p - \left(\frac{\partial p}{\partial T}\right)_{\rho_i}\mathrm{d}T - \sum_{i=1}^{N-1}\rho\left[\left(\frac{\partial p}{\partial \rho_i}\right)_{T,\rho_{j\neq i}} - \left(\frac{\partial p}{\partial \rho_N}\right)_{T,\rho_{j\neq N}}\right]\mathrm{d}Y_i\right\}\Bigg/\left(\frac{\partial p}{\partial \rho}\right)_{T,Y_i}. \tag{3.14}$$

Eqs. (3.13) and (3.14) can be combined with Eq. (3.9) to establish an important thermodynamic relationship for enthalpy

$$\mathrm{d}h = B_T\,\mathrm{d}T + B_p\,\mathrm{d}p + \sum_{i=1}^{N-1} B_{Y_i}\,\mathrm{d}Y_i, \tag{3.15a}$$

where the coefficients B_T, B_p, and B_{Y_i} are defined as

$$B_T = C_v - \frac{1}{\rho}\left(\frac{\partial p}{\partial T}\right)_{\rho_i}\left(\frac{\partial \rho}{\partial p}\right)_{T,Y_i}\left(\sum_{i=1}^{N} Y_i\tilde{e}_i - e - \frac{p}{\rho}\right), \tag{3.15b}$$

$$B_p = \frac{1}{\rho} + \frac{1}{\rho}\left(\frac{\partial \rho}{\partial p}\right)_{T,Y_i}\left(\sum_{i=1}^{N} Y_i\tilde{e}_i - e - \frac{p}{\rho}\right), \tag{3.15c}$$

$$B_{Y_i} = (\tilde{e}_i - \tilde{e}_N) - \left(\frac{\partial \rho}{\partial p}\right)_{T,Y_i}\left(\sum_{i=1}^{N} Y_i\tilde{e}_i - e - \frac{p}{\rho}\right)\left[\left(\frac{\partial p}{\partial \rho_i}\right)_{T,\rho_{j\neq i}} - \left(\frac{\partial p}{\partial \rho_N}\right)_{T,\rho_{j\neq N}}\right]. \tag{3.15d}$$

The coefficient, B_T, is equivalent to the constant-pressure heat capacity, C_p, of a fluid mixture, according to its definition. Thus,

$$C_p = B_T = C_v - \frac{1}{\rho}\left(\frac{\partial p}{\partial T}\right)_{\rho_i}\left(\frac{\partial \rho}{\partial p}\right)_{T,Y_i}\left(\sum_{i=1}^{N} Y_i\tilde{e}_i - e - \frac{p}{\rho}\right). \tag{3.16}$$

3.3. Speed of sound

In this section, we will derive a thermodynamic relationship for calculating the speed of sound in a general fluid mixture, defined as

$$a^2 = \left(\frac{\partial p}{\partial \rho}\right)_{s,Y_i}. \tag{3.17}$$

We start with the following relationship by rewriting Eq. (3.14):

$$\mathrm{d}p = \left(\frac{\partial p}{\partial T}\right)_{\rho_i}\mathrm{d}T + \sum_{i=1}^{N-1}\rho\left[\left(\frac{\partial p}{\partial \rho_i}\right)_{T,\rho_{j\neq i}} - \left(\frac{\partial p}{\partial \rho_N}\right)_{T,\rho_{j\neq N}}\right]\mathrm{d}Y_i + \left(\frac{\partial p}{\partial \rho}\right)_{T,Y_i}\mathrm{d}\rho. \tag{3.18}$$

A relationship can be easily derived from Eq. (3.18) as

$$\left(\frac{\partial p}{\partial \rho}\right)_{s,Y_i} = \left(\frac{\partial p}{\partial T}\right)_{\rho_i}\left(\frac{\partial T}{\partial \rho}\right)_{s,Y_i} + \left(\frac{\partial p}{\partial \rho}\right)_{T,Y_i}. \tag{3.19}$$

In thermodynamics, the following relationship exists:

$$s = s(T, \rho, Y_i), \quad i = 1, \ldots, N-1. \tag{3.20}$$

Its differential form can be written as

$$\mathrm{d}s = \frac{C_v}{T}\,\mathrm{d}T - \frac{1}{\rho^2}\left(\frac{\partial p}{\partial T}\right)_{\rho_i}\mathrm{d}\rho + \sum_{i=1}^{N-1}\left(\frac{\partial s}{\partial Y_i}\right)_{T,\rho,Y_{j\neq i}}\mathrm{d}Y_i. \tag{3.21}$$

In deriving Eq. (3.21), we have applied the definitions of the constant-volume heat capacity, Eq. (3.22a), and a Maxwell relation [10], Eq. (3.22b),

$$C_v = \left(\frac{\partial e}{\partial T}\right)_{\rho,Y_i} = \left(\frac{T\partial s}{\partial T}\right)_{\rho,Y_i}, \tag{3.22a}$$

$$\left(\frac{\partial s}{\partial \rho}\right)_{T,Y_i} = -\frac{1}{\rho^2}\left(\frac{\partial p}{\partial T}\right)_{\rho_i}. \tag{3.22b}$$

Based on Eq. (3.21), the following thermodynamic relationship can be easily found:

$$\left(\frac{\partial T}{\partial \rho}\right)_{s,Y_i} = \frac{T}{\rho^2}\left(\frac{\partial p}{\partial T}\right)_{\rho_i} \Big/ C_v. \tag{3.23}$$

Substitution of Eq. (3.23) into Eq. (3.19) yields an expression for the speed of sound in a general fluid mixture

$$a^2 = \left(\frac{\partial p}{\partial \rho}\right)_{s,Y_i} = \frac{C_p}{C_v}\left(\frac{\partial p}{\partial \rho}\right)_{T,Y_i}. \tag{3.24}$$

4. Thermodynamic properties based on Soave–Redlich–Kwong (SRK) equation of state

The thermodynamic relations derived in the preceding section are general and valid for any equation of state. As a specific example, a modified Soave–Redlich–Kwong (SRK) equation of state [11,12] is employed herein because of its broad use in treating fluid p–V–T behavior over a broad range of thermodynamic states, except for the near-critical regime, where a more accurate equation of state, such as the Benedict–Webb–Rubin (BWR) equation of state, is required [1,13].

4.1. Soave–Redlich–Kwong (SRK) equation of state

The Soave–Redlich–Kwong (SRK) equation of state takes the form

$$p = \frac{\rho R_u T}{(M_w - b\rho)} - \frac{a\alpha}{M_w}\frac{\rho^2}{(M_w + b\rho)}, \tag{4.1}$$

where R_u is the universal gas constant and M_w the molecular weight of a fluid mixture. The two parameters, a and b, accounting for the effects of attractive and repulsive forces among molecules, respectively, are calculated using the following mixing rules:

$$\alpha a = \sum_{i=1}^{N}\sum_{j=1}^{N} x_i x_j \alpha_{ij} a_{ij}, \tag{4.2}$$

$$b = \sum_{i=1}^{N} x_i b_i, \tag{4.3}$$

where x_i is the mole fraction of species i. The parameter $\alpha_{ij}a_{ij}$ is given as

$$\alpha_{ij}a_{ij} = \sqrt{\alpha_i\alpha_j a_i a_j}(1-\kappa_{ij}), \tag{4.4}$$

where κ_{ij} is a binary interaction coefficient. The coefficients, a_i and b_i, are determined from the following universal relationships:

$$a_i = 0.42747\frac{R_u^2 T_{ci}^2}{p_{ci}}, \tag{4.5}$$

$$b_i = 0.08664\frac{R_u T_{ci}}{p_{ci}}, \tag{4.6}$$

where T_{ci} and p_{ci} are the critical temperature and pressure of species i, respectively. The third parameter in Eq. (4.4), α_i, is given as

$$\alpha_i = \left[1 + S_i\left(1-\sqrt{T_{ri}}\right)\right]^2, \tag{4.7}$$

where T_{ri} is the reduced temperature of species i, defined as

$$T_{ri} = \frac{T}{T_{ci}} \tag{4.8}$$

and S_i is a function of the acentric factor ω_i

$$S_i = 0.48508 + 1.5517\omega_i - 0.15613\omega_i^2. \tag{4.9}$$

For a quantum gas such as hydrogen, Eq. (4.7) is modified as [12]

$$\alpha_{H_2} = 1.202\exp(-0.30228T_r). \tag{4.10}$$

This equation is accurate for reduced temperatures above 2.5. Since the critical temperature of hydrogen is 33.2 K, it is applicable for most of hydrogen mixtures of practical interest. When Eq. (4.10) is used, the binary interaction coefficient, κ_{ij}, involving hydrogen should be set to zero.

4.2. Thermodynamic relations based on SRK equation of state

Based on the Soave–Redlich–Kwong (SRK) equation of state, the following differential expressions, used extensively in the numerical treatment of general fluid mixtures, can be derived as:

$$\left(\frac{\partial p}{\partial T}\right)_{\rho_j} = \frac{\rho R_u}{(M_w - b\rho)} - \frac{1}{M_w}\left[\frac{\partial}{\partial T}(a\alpha)\right]_{\rho,Y_i}\frac{\rho^2}{(M_w + b\rho)}, \tag{4.11}$$

$$\left(\frac{\partial p}{\partial \rho}\right)_{T,Y_i} = \frac{M_w R_u T}{(M_w - b\rho)^2} - \frac{a\alpha}{M_w}\frac{\rho(2M_w + b\rho)}{(M_w + b\rho)^2}, \tag{4.12}$$

$$\left(\frac{\partial p}{\partial \rho_i}\right)_{T,\rho_{j\neq i}} = \frac{M_w R_u T}{M_{w_i}(M_w - b\rho)^2}[M_w + \rho(b_i - b)] - \frac{2\rho\sum_j x_j a_{ij}\alpha_{ij}}{M_{w_i}(M_w + b\rho)} + \frac{a\alpha\rho^2 b_i}{M_{w_i}(M_w + b\rho)^2} \tag{4.13}$$

where the explicit expression for $\partial(a\alpha)/\partial T$ is given in Appendix C. The partial-density internal energy of species i, $\tilde{e}_i$, required in the thermodynamic relations in Eqs. (3.10a)–(3.10e), (3.15a)–(3.15d) and (3.16), needs to be derived. We start with the following expression for the specific internal energy, e:

$$e(T,\rho) = e_0(T) + \int_0^{\rho} \left[\frac{p}{\rho^2} - \frac{T}{\rho^2} \left(\frac{\partial p}{\partial T} \right)_{\rho} \right]_T \mathrm{d}\rho, \tag{4.14}$$

where the subscript 0 represents a reference thermodynamic state at a low pressure with a negligible reference density. With the application of Eqs. (4.1) and (4.11), Eq. (4.14) can be integrated to yield

$$e(T,\rho) = e_0(T) + \frac{T^2}{bM_{\mathrm{w}}} \left(\frac{\partial (a\alpha/T)}{\partial T} \right)_{\rho,Y_i} \ln\left(1 + \frac{b\rho}{M_{\mathrm{w}}}\right). \tag{4.15}$$

Substitution of Eq. (4.15) into Eq. (3.3) establishes the following equation for the partial-density internal energy of species i:

$$\begin{aligned} \tilde{e}_i = e_{i,0} &+ \frac{2}{bM_{\mathrm{w}_i}} \left[\sum_j x_j \left(T \frac{\partial}{\partial T} (a_{ij}\alpha_{ij}) - a_{ij}\alpha_{ij} \right) \right] \ln\left(1 + \frac{b\rho}{M_{\mathrm{w}}}\right) \\ &+ \frac{b_i}{bM_{\mathrm{w}_i}} \left[T \frac{\partial}{\partial T} (a\alpha) - a\alpha \right] \left[\frac{\rho}{M_{\mathrm{w}} + b\rho} - \frac{1}{b} \ln\left(1 + \frac{b\rho}{M_{\mathrm{w}}}\right) \right]. \end{aligned} \tag{4.16}$$

The following relationship exists in thermodynamics:

$$\rho h = \rho e + p. \tag{4.17}$$

Taking the derivative of the partial density of species i on both sides of Eq. (4.17), with the temperature and all the other partial densities remaining constant, leads to

$$\left(\frac{\partial \rho h}{\partial \rho_i} \right)_{T,\rho_{j\neq i}} = \left(\frac{\partial \rho e}{\partial \rho_i} \right)_{T,\rho_{j\neq i}} + \left(\frac{\partial p}{\partial \rho_i} \right)_{T,\rho_{j\neq i}}. \tag{4.18a}$$

According to the definition of partial-density property given in Eq. (2.16), we have

$$\tilde{h}_i = \tilde{e}_i + \left(\frac{\partial p}{\partial \rho_i} \right)_{T,\rho_{j\neq i}}. \tag{4.18b}$$

Substitution of the above equation into Eq. (2.18), a relationship for partial-mass enthalpy, $\bar{h}_i$, is derived as

$$\bar{h}_i = \tilde{e}_i + \left(\frac{\partial p}{\partial \rho_i} \right)_{T,\rho_{j\neq i}} \left[1 - \rho \left(\frac{\partial h}{\partial p} \right)_{T,Y_j} \right]. \tag{4.19}$$

Eq. (4.19) can be further simplified by means of Eq. (3.15a).

$$\bar{h}_i = \tilde{e}_i + \left(\frac{\partial p}{\partial \rho_i} \right)_{T,\rho_{j\neq i}} [1 - \rho B_p]. \tag{4.20}$$

The definition of constant-volume heat capacity is given as

$$C_v = \left(\frac{\partial e}{\partial T} \right)_{\rho,Y_i}. \tag{4.21a}$$

Substitution of Eq. (4.15) into Eq. (4.21a) yields the following formula for calculating constant-volume heat capacity:

$$C_v = C_{v,0} + \frac{T}{bM_{\mathrm{w}}} \frac{\partial^2}{\partial T^2} (a\alpha) \ln\left(1 + \frac{b\rho}{M_{\mathrm{w}}}\right). \tag{4.21b}$$

An explicit expression for $\partial^2(a\alpha)/\partial T^2$ is given in Appendix C. The constant-pressure heat capacity can be determined using the fundamental thermodynamic relationship

$$C_p = C_v + \frac{T}{\rho^2}\left(\frac{\partial p}{\partial T}\right)^2_{\rho_i} \Bigg/ \left(\frac{\partial p}{\partial \rho}\right)_{T,Y_i}. \tag{4.22}$$

5. Numerical treatment

5.1. Preconditioning scheme

As mentioned in Section 2.1, eigenvalue disparity poses a serious numerical challenge in solving low-speed fluid flows. In order to circumvent this numerical difficulty, a pseudo-time derivative of the form, $\Gamma\partial\hat{Q}/\partial\tau$, is added into the conservation equations, following the strategy described in [8,9]. The preconditioning matrix Γ and the pseudo-time variable vector $\hat{Q}$ are chosen as

$$\Gamma = \begin{bmatrix} 1/\beta & 0 & 0 & 0 & 0 & \cdots & 0 \\ u/\beta & \rho & 0 & 0 & 0 & \cdots & 0 \\ v/\beta & 0 & \rho & 0 & 0 & \cdots & 0 \\ h_t/\beta - 1 & \rho u & \rho v & \rho & 0 & \cdots & 0 \\ Y_1/\beta & 0 & 0 & 0 & \rho & \cdots & 0 \\ \vdots & \vdots & \vdots & \vdots & \vdots & \ddots & 0 \\ Y_{N-1}/\beta & 0 & 0 & 0 & 0 & \cdots & \rho \end{bmatrix}, \tag{5.1}$$

$$\hat{Q} = y^{\delta}[p_g \quad u \quad v \quad h \quad Y_i]^{\mathrm{T}}, \tag{5.2}$$

where β is a scaling parameter and τ is the pseudo-time. To facilitate numerical treatment, the viscous flux vectors in Eqs. (2.6) and (2.7), E_v and F_v, are further written in second-order terms,

$$E_v = y^{\delta}\left(R_{xx}\frac{\partial Q_v}{\partial x} + R_{xy}\frac{\partial Q_v}{\partial y}\right), \tag{5.3}$$

$$F_v = y^{\delta}\left(R_{yx}\frac{\partial Q_v}{\partial x} + R_{yy}\frac{\partial Q_v}{\partial y}\right), \tag{5.4}$$

where the viscous vector Q_v is defined as

$$Q_v = [p_g \quad u \quad v \quad T \quad Y_i]^{\mathrm{T}}. \tag{5.5}$$

The viscous coefficient matrices in Eqs. (5.3) and (5.4), R_{xx}, R_{xy}, R_{yx}, and R_{yy}, are given in Appendix A. The conservation equations with the preconditioning term can now be expressed as

$$\Gamma\frac{\partial\hat{Q}}{\partial\tau} + \frac{\partial Q}{\partial t} + \frac{\partial E}{\partial x} + \frac{\partial F}{\partial y} - \frac{\partial}{\partial x}\left[y^{\delta}R_{xx}\frac{\partial Q_v}{\partial x} + y^{\delta}R_{xy}\frac{\partial Q_v}{\partial y}\right] - \frac{\partial}{\partial y}\left[y^{\delta}R_{yx}\frac{\partial Q_v}{\partial x} + y^{\delta}R_{yy}\frac{\partial Q_v}{\partial y}\right] = S. \tag{5.6}$$

An implicit dual time-stepping integration technique is employed to solve the discretized conservation equations

$$\left[\Gamma-\Delta\tau D+\frac{a_1\Delta\tau}{\Delta t}T+\Delta\tau\frac{\partial}{\partial x}A+\Delta\tau\frac{\partial}{\partial y}B-\Delta\tau\frac{\partial}{\partial x}\left(y^{\delta}\hat{R}_{xx}\frac{\partial}{\partial x}\left(\frac{1}{y^{\delta}}\right)\right)-\Delta\tau\frac{\partial}{\partial y}\left(y^{\delta}\hat{R}_{yy}\frac{\partial}{\partial y}\left(\frac{1}{y^{\delta}}\right)\right)-\Delta\tau D_i^{(2)}\right]\Delta\hat{Q}$$
$$=\Delta\tau\left(S^p-\frac{a_1Q^p+a_2Q^n+a_3Q^{n-1}}{\Delta t}-\frac{\partial(E-E_v)^p}{\partial x}+\frac{\partial(F-F_v)^p}{\partial y}+D_{\mathrm{e}}^{(2)}-D_{\mathrm{e}}^{(4)}\right), \tag{5.7}$$

where T, D, A, B, $\hat{R}_{xx}$, and $\hat{R}_{rr}$ are the Jacobian matrices defined as follows:

$$T=\frac{\partial Q}{\partial\hat{Q}}, \tag{5.8a}$$

$$A=\frac{\partial E}{\partial\hat{Q}}, \tag{5.8b}$$

$$B=\frac{\partial F}{\partial\hat{Q}}, \tag{5.8c}$$

$$D=\frac{\partial S}{\partial\hat{Q}}, \tag{5.8d}$$

$$\hat{R}_{xx}=R_{xx}\frac{\partial Q_v}{\partial(\hat{Q}/y^{\delta})}, \tag{5.8e}$$

$$\hat{R}_{yy}=R_{yy}\frac{\partial Q_v}{\partial(\hat{Q}/y^{\delta})}. \tag{5.8f}$$

The superscripts $n-1$, n, and $n+1$ represent the previous, current, and next physical time step, respectively. The coefficients, a_1, a_2, and a_3 on the right-hand side of Eq. (5.7), are chosen based on the requirement of temporal accuracy. The left-hand side of Eq. (5.7) is evaluated in pseudo-time. Once a converged solution is reached during pseudo-time iterations, the solution in the physical time step $n+1$ is updated.

A second-order time-accurate scheme is implemented in the present case, with the coefficients a_1, a_2, and a_3 chosen as 3/2, −2, and 1/2, respectively. Spatial discretizaiton is achieved using a second-order central-differencing scheme. Artificial dissipation is added to Eq. (5.7) to enhance numerical stability and convergence, in which $D_i^{(2)}$ represents an implicit second-order artificial viscous term, and $D_{\mathrm{e}}^{(2)}$ and $D_{\mathrm{e}}^{(4)}$ explicit second- and fourth-order artificial viscous terms, respectively. All of the artificial viscous terms contain components in both the axial and vertical directions, respectively. For example, the explicit second-order artificial viscous term can be expressed as

$$D_{\mathrm{e}}^{(2)}=D_{\mathrm{ex}}^{(2)}+D_{\mathrm{ey}}^{(2)}, \tag{5.9}$$

where

$$D_{\mathrm{ex}}^{(2)}=\Gamma\nabla_x\left(\varepsilon_{\mathrm{ex}}^{(2)}|\lambda_{\mathrm{A}}|y^{\delta}\right)\Delta_x(\hat{Q}). \tag{5.10}$$

The symbols Δ and ∇ represent the standard forward and backward differences, respectively, and λ_{A} the maximum eigenvalue in the axial direction. The coefficient $\varepsilon_{\mathrm{ex}\,i+1/2,j}^{(2)}$ is defined as

$$\varepsilon_{\mathrm{ex}\,i+1/2,j}^{(2)}=K^{(2)}\max\left(\psi_{i,j}^{(x)},\psi_{i+1,j}^{(x)}\right). \tag{5.11}$$

The explicit second-order artificial viscous term is only needed in regions with sharp discontinuities, and vanishes in the smooth domain. A discontinuity detector is, therefore, defined as

$$\psi_{i,j}^{(x)} = \frac{|\rho_{i+1,j} - 2\rho_{i,j} + \rho_{i-1,j}|}{(1-\omega)(|\rho_{i+1,j} - \rho_{i,j}| + |\rho_{i,j} - \rho_{i-1,j}|) + \omega(\rho_{i+1,j} + 2\rho_{i,j} + \rho_{i-1,j})}. \tag{5.12}$$

Density is often chosen over pressure in Eq. (5.12) because of its superior performance in identifying a fluid-state discontinuity. The constant coefficients, $K^{(2)}$ and ω, are generally set to 0.5 and 0.1, respectively.

Similarly, the x-component of the explicit fourth-order artificial viscous term is defined as

$$D_{\mathrm{ex}}^{(4)} = \Gamma\nabla_x\left(\varepsilon_{\mathrm{ex}}^{(4)}|\lambda_{\mathrm{A}}|y^{\delta}\right)\Delta_x\nabla_x\Delta_x(\hat{Q}), \tag{5.13}$$

where the coefficient, $\varepsilon_{\mathrm{ex}\ i+1/2,j}^{(4)}$, is defined as

$$\varepsilon_{\mathrm{ex}\ i+1/2,j}^{(4)} = \max\left(0, K^{(4)} - \varepsilon_{\mathrm{ex}\ i+1/2,j}^{(2)}\right). \tag{5.14}$$

The constant coefficient, $K^{(4)}$, is set to 1/32. This approach guarantees that the second-order artificial viscous terms exert their influence in regions with strong gradients, whereas in other smooth locations, only the fourth-order terms exist. The implicit artificial viscous term on the left-hand side of Eq. (5.7) is employed solely for the purpose of numerical stability. Its x-component takes the form

$$D_{ix}^{(2)} = \Gamma\nabla_x\left(\varepsilon_{ix}^{(2)}|\lambda_{\mathrm{A}}|y^{\delta}\right)\Delta_x\left(\frac{1}{y^{\delta}}\right), \tag{5.15}$$

where the viscous coefficient, $\varepsilon_{ix}^{(2)}$, is defined as

$$\varepsilon_{ix\ i+1/2,j}^{(2)} = \max\left(\varepsilon_{\mathrm{ex}\ i+1/2,j}^{(2)}, 2\varepsilon_{\mathrm{ex}\ i+1/2,j}^{(4)}\right). \tag{5.16}$$

Other details regarding artificial viscous terms and TVD schemes are discussed in [14,15]. A modified strongly implicit procedure (MSIP), originally developed by Schneider and Zedan [16], is implemented in the present work to solve the resultant linear algebraic equations.

5.2. Jacobians matrices

The thermodynamic relations developed in Section 3 will be applied to derive numerical Jacobian matrices. For example, the expression for enthalpy as a function of density, pressure, and mass fraction, Eq. (3.10e), is required to obtain the Jacobian matrix A in Eq. (5.8b). The explicit expressions for Jacobian matrices are given in Appendix B.

5.3. Eigenvalues

The eigenvalues need to be examined in order to obtain direct insight into the numerical characteristics of the present scheme, especially the convergence and robustness properties. The eigenvalues associated with the matrix, $\Gamma^{-1}A$, in the axial direction are

$$\lambda_{\mathrm{A}} = u, \frac{1}{2}\left[u\left(1+\frac{\beta}{a_c^2}\right) \pm \sqrt{u^2\left(1-\frac{\beta}{a_c^2}\right)^2 + 4\beta}\right], u, u, \ldots, u, \tag{5.17}$$

where a_c is given as

$$a_c^2 = \frac{A_\rho}{1/\rho - A_p}. \tag{5.18}$$

The variables, A_p and A_ρ, are given in Eqs. (3.10b) and (3.10c), respectively. The latter can be further expressed as

$$\begin{aligned} A_\rho &= -C_v\left(\frac{\partial T}{\partial p}\right)_{\rho_i}\left(\frac{\partial p}{\partial \rho}\right)_{T,Y_i} + \frac{1}{\rho}\sum_{i=1}^{N} Y_i\tilde{e}_i - \frac{e}{\rho} - \frac{p}{\rho^2} \\ &= -\left(\frac{\partial T}{\partial p}\right)_{\rho_i}\left(\frac{\partial p}{\partial \rho}\right)_{T,Y_i}\left[C_v - \frac{1}{\rho}\left(\frac{\partial p}{\partial T}\right)_{\rho_i}\left(\frac{\partial \rho}{\partial p}\right)_{T,Y_i}\left(\sum_{i=1}^{N} Y_i\tilde{e}_i - e - \frac{p}{\rho}\right)\right]. \end{aligned} \tag{5.19}$$

As developed in Eq. (3.16), the last term in the bracket on the right-hand side is the constant-pressure heat capacity, C_p, leading to

$$A_\rho = -\left(\frac{\partial T}{\partial p}\right)_{\rho_i}\left(\frac{\partial p}{\partial \rho}\right)_{T,Y_i} C_p. \tag{5.20}$$

Eq. (3.10b) can be rewritten as

$$\frac{1}{\rho} - A_p = -C_v\left(\frac{\partial T}{\partial p}\right)_{\rho_i}. \tag{5.21}$$

Substitute Eqs. (5.20) and (5.21) into Eq. (5.18) to obtain

$$a_c^2 = -\left(\frac{\partial T}{\partial p}\right)_{\rho_i}\left(\frac{\partial p}{\partial \rho}\right)_{T,Y_i} C_p \Big/ -C_v\left(\frac{\partial T}{\partial p}\right)_{\rho_i} = \frac{C_p}{C_v}\left(\frac{\partial p}{\partial \rho}\right)_{T,Y_i} = a^2. \tag{5.22}$$

Now the eigenvalues can be determined as

$$\lambda_{\mathrm{A}} = u, \frac{1}{2}\left[u\left(1+\frac{\beta}{a^2}\right) \pm \sqrt{u^2\left(1-\frac{\beta}{a^2}\right)^2 + 4\beta}\ \right], u, u, \ldots, u \tag{5.23}$$

which are identical to those obtained in [8,9] for ideal gas mixtures.

5.4. Scaling factor

A proper scaling factor is required to circumvent the numerical difficulty arising from eigenvalue disparity. For inviscid fluid flows, it is chosen as [8,9,17,18]

$$\beta_{\mathrm{inv}} = \begin{cases} u_{\mathrm{R}}^2 & \text{if } u^2 < u_{\mathrm{R}}^2, \\ u^2 & \text{if } u_{\mathrm{R}}^2 < u^2 < a^2, \\ a^2 & \text{if } u^2 > a^2, \end{cases} \tag{5.24}$$

where u_{R} is a reference velocity of small value. The scaling factor in Eq. (5.24) renders the eigenvalues of the system the same order of magnitude for all-speed fluid flows. Furthermore, since all the eigenvalues remain as real numbers, the preconditioned conservation equations maintain the hyperbolic characteristics.

Implementation of the scaling factor given in Eq. (5.24) alone, however, is not sufficient for treating viscous fluid flows, especially when viscous diffusion overrides convection in regions where viscous shear stress prevails. A proper scaling factor capable of controlling both viscous diffusion and convection is thus used as follows [8,9,17,18]:

$$\beta = \min(1, \max(\beta_{\text{inv}}, \beta_{\text{vis}})). \tag{5.25}$$

The inviscid scaling factor, β_{inv}, is used to rescale the wave propagation and convective processes, whereas the viscous scaling factor, β_{vis}, is used for the viscous damping effect. Details about these scaling factors can be found in [18].

6. Test cases

The thermodynamics treatment and numerical scheme development in the preceding sections are validated against several test problems involving supercritical droplet vaporization in both quiescent and convective environments. Results demonstrate the efficiency and robustness of the algorithm in treating fluid flows over a broad range of thermodynamic states.

6.1. Evaluation of transport properties

Transport properties play an important role in determining fluid dynamics. The fluid thermal conductivity and viscosity can be evaluated by means of an extended corresponding-state principle detailed in [19,20]. Special attention is given to the effects of pressure on transport properties, including the abnormal variations near the thermodynamic critical mixing point. Estimation of mass diffusivity poses a serious challenge because of the lack of a formal theory or even a theoretically based correlation. Takahashi [21] suggested a simple scheme for predicting the binary mass diffusivity of a dense fluid by means of a corresponding-state approach. The method appears to be the most complete to date and has demonstrated moderate success in the limited number of tests conducted [1].

6.2. Droplet vaporization in quiescent environment

Several numerical and experimental investigations of supercritical droplet vaporization in a quiescent environment have been conducted [1], making it a suitable case for numerical model validation. The physical model chosen here includes an *n*-heptane droplet vaporizing in high-pressure nitrogen gas. The process can be approximated as one-dimensional because of spherical symmetry. The droplet initially has a diameter of 700 μm and a uniform temperature of 300 K. The ambient nitrogen temperature is 750 K. A total of 160 grids proves to be sufficient to resolve the vaporization process. An increase in the grid number from 160 to 300 shows little difference in the calculated temperature and mass-fraction distributions, as shown in Fig. 1. The experimental data of Nomura et al. [22] are presented for comparison with the numerical results. Fig. 2 shows the temporal evolution of droplet diameter squared at an ambient pressure of 0.5 MPa at temperatures of 660 and 750 K. Reasonable agreement is obtained between the experimental and numerical data, given the uncertainties involved in the measurements. The droplet first expands, in the early stage of its lifetime, due to the volume dilation arising from the heat transfer from the surrounding gas. Fig. 3 shows the result for a higher pressure of 2 MPa and an ambient temperature of 660 K. The numerical result agrees closely with experimental data during the first part of the vaporization process, but then deviates substantially at the end. Several reasons causing such a discrepancy have been identified. First, a computer-aided image analysis system was employed in the experiments. Since the droplet deforms rapidly with diminishing surface tension as it heats up, a visual definition of the droplet diameter inevitably gives rise to considerable uncertainty, especially when the droplet size becomes small at the end of its lifetime. Second, the droplets were suspended using a fiber, while a floating droplet was used in numerical simulations. Morin [23] recently indicated that the effect of suspension fiber increases with increasing pressure and temperature, and must be taken into account when analyzing droplet behavior. Third, the

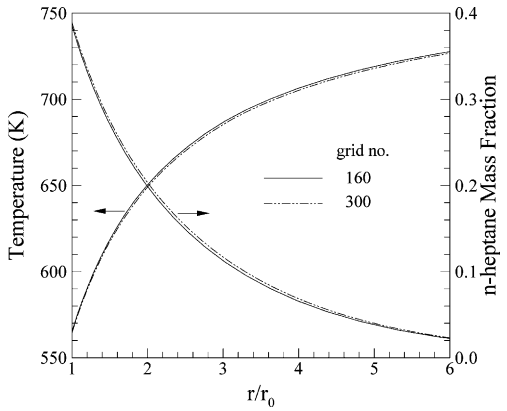

Fig. 1. Effect of grid resolution on calculated temperature and mass-fraction of *n*-heptane droplet vaporization in quiescent nitrogen ($T_\infty = 750$ K, $p_\infty = 5$ MPa).

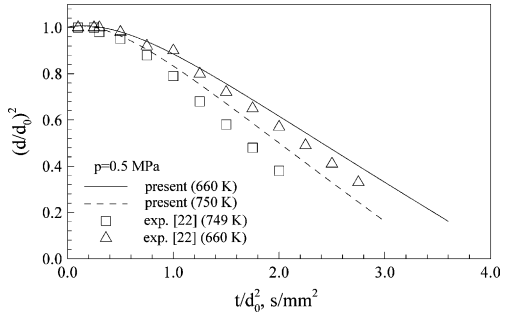

Fig. 2. Temporal evolution of droplet diameter squared; *n*-heptane droplet vaporization in quiescent nitrogen ($p_\infty = 0.5$ MPa).

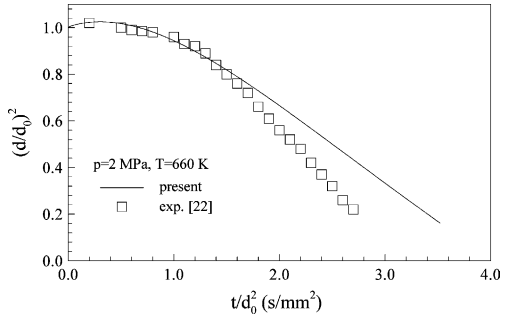

Fig. 3. Temporal evolution of droplet diameter squared; *n*-heptane droplet vaporization in quiescent nitrogen ($p_\infty = 2.0$ MPa).

influence of buoyancy-induced natural convection on droplet vaporization rate needs to be considered, even in the microgravity environment adopted in the experiments [24]. In spite of the discrepancy with experimental measurements, the present algorithm shows a correct trend and thus can be effectively used to study general fluid behavior at high pressures.

The distributions of temperature and mass fraction in the droplet interior and the surrounding gases are presented in Figs. 4 and 5 for three different pressures of 10, 30, and 50 atm. Since the critical pressure of *n*-heptane is 27.3 atm, the first case corresponds to subcritical vaporization, and the last two cases to supercritical conditions. The effect of pressure on the droplet is clearly observed.

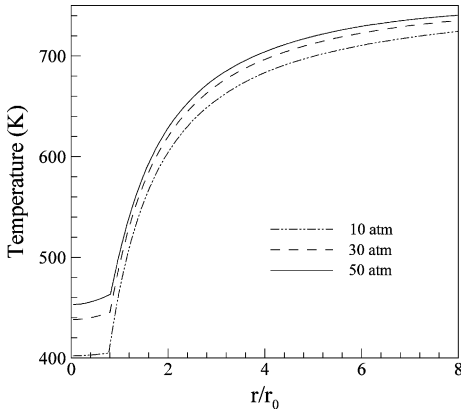

Fig. 4. Temperature distributions at various ambient pressures; *n*-heptane droplet vaporization in quiescent nitrogen ($T_\infty = 750$ K).

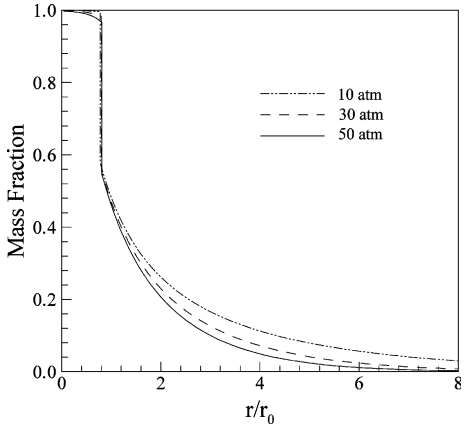

Fig. 5. *n*-Heptane mass-fraction distributions at various ambient pressures; *n*-heptane droplet vaporization in quiescent nitrogen ($T_\infty = 750$ K).

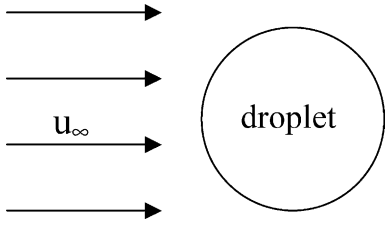

Fig. 6. Single droplet vaporization in convective environment under supercritical condition.

6.3. Supercritical droplet vaporization in convective environments

Droplet vaporization in a supercritical convective environment represents a more challenging problem for numerical simulation. In the present study, an oxygen droplet, initially with a diameter of 50 μm and a uniform temperature distribution of 100 K, is suddenly introduced to a hydrogen stream, as shown

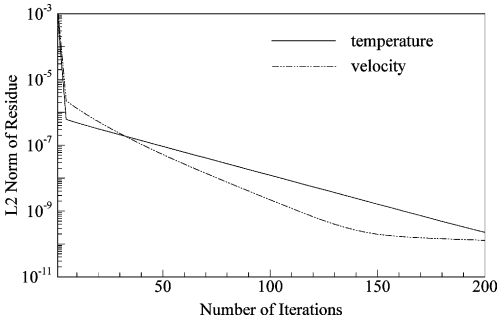

Fig. 7. Numerical convergence history for liquid oxygen droplet vaporization in supercritical hydrogen stream ($p_\infty = 100$ atm, $T_\infty = 1000$ K).

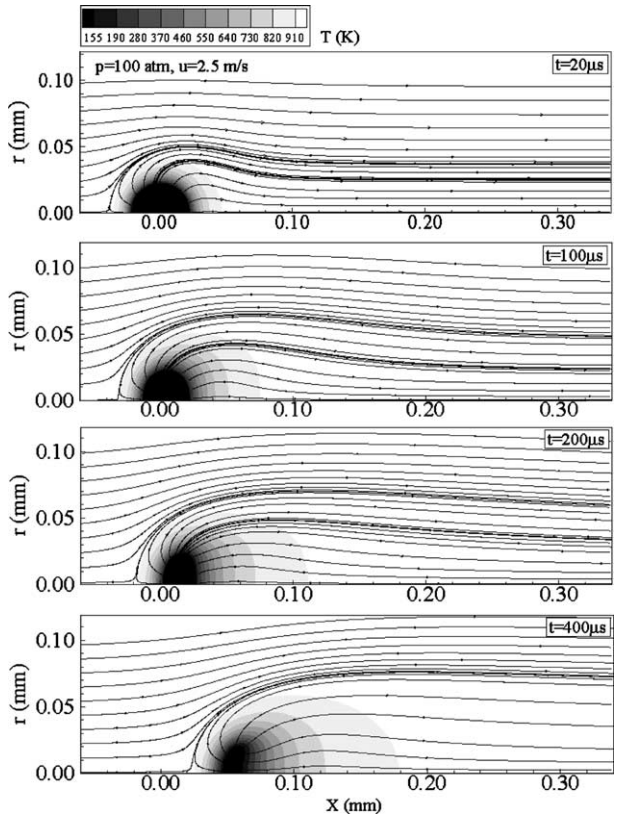

Fig. 8. Temporal evolution of temperature and flow fields; liquid oxygen droplet vaporization in supercritical hydrogen stream ($p_\infty = 100$ atm, $T_\infty = 1000$ K, $u_\infty = 2.5$ m/s).

schematically in Fig. 6. The freestream pressure and temperature are 100 atm and 1000 K, respectively. The initial density of oxygen droplet is 1200 kg/m^3, whereas the ambient hydrogen density is 2.4 kg/m^3, resulting in a density of 500:1. A grid independence study was first conducted to assess numerical accuracy. The result indicates that a grid of 201 × 71 points, clustered near the droplet surface and within the droplet interior, is sufficient to provide accurate resolution of the droplet behavior. An increase of grid resolution to 253 × 99 points causes less than 3% increase in the droplet lifetime. Fig. 7 shows a typical convergence history of the inner iteration in the pseudo-time domain. The residual errors decrease by ten orders of magnitude within 200 iterations, beyond which no further convergence is obtained because of low-frequency numerical errors. The method proposed by Venkateswaran and Merkle [25] may be implemented to achieve a better convergence rate. The present algorithm, however, is sufficient for transient calculations since the residual errors can be reduced by three orders of magnitude with only a small number of iterations.

The temporal evolutions of the flow and temperature fields are given in Figs. 8 and 9, where the reference coordinates move with the average droplet velocities. Fig. 8 provides information about the case with a hydrogen velocity of 2.5 m/s and a pressure 100 atm. The corresponding Reynolds number (Re) based on the initial droplet diameter, d_0, freestream velocity, u_0, and ambient properties is 15. In such a low Reynolds-number case, the hydrogen flow passes over the droplet smoothly, and no flow separation

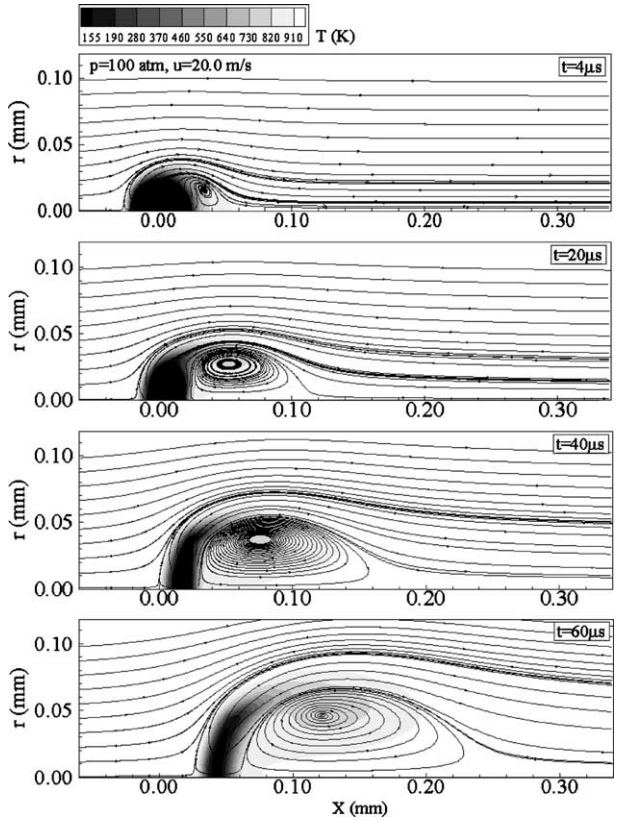

Fig. 9. Temporal evolution of temperature and flow fields; liquid oxygen droplet vaporization in supercritical hydrogen stream ($p_\infty = 100$ atm, $T_\infty = 1000$ K, $u_\infty = 20$ m/s).

occurs behind the droplet. When the incoming velocity increases to 20 m/s (i.e., $Re = 120$), the flow becomes detached from the droplet surface, producing a separation bubble in the wake of the droplet, as shown in Fig. 9. The bubble continues to grow as a result of droplet deformation throughout its entire lifetime. Fig. 10 shows the vorticity fields at various freestream conditions. The maximum vorticity occurs near the front top region of the droplet, with its magnitude increasing with both the incoming velocity and pressure, a phenomenon that can be easily explained with the increased Reynolds number. Fig. 11 presents the temperature field for the case with a freestream velocity of 20 m/s and pressure of 100 atm. The low temperature region corresponds to the droplet interior. The droplet deforms slightly in the direction perpendicular to the flow at $t = 20\,\mu s$, and becomes an oblate with an intense stretching near the tip. When the time elapses to 40 μs, the droplet is further extended in the cross-flow direction, and the tip region is stretched downstream. It then bent severely to form a crescent shape at the end of the vaporization process.

The distributions of oxygen mass fraction are shown in Fig. 12 for four different cases. The extent to which the droplet deforms increases with the incoming flow velocity. The droplet may deform to a simple oblate, a bent oblate with indentation in the back, or a crescent shape with strong stretching at the tip, depending on the freestream conditions. In general, the droplet deformation becomes more severe at a higher pressure due to its effect on the Reynolds number, which increases with increasing pressure.

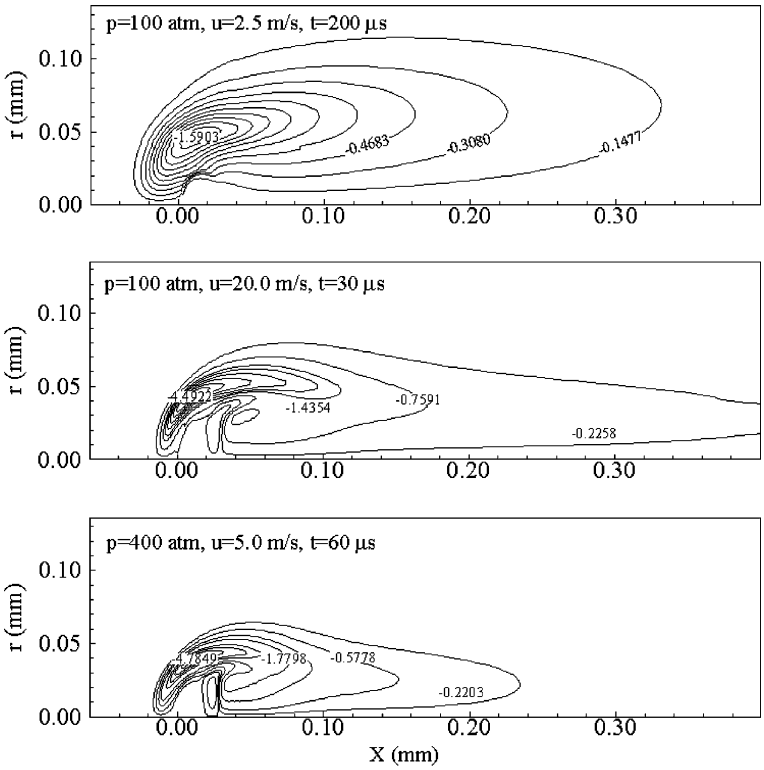

Fig. 10. Temporal evolution of vorticity field at various ambient conditions; liquid oxygen droplet vaporization in supercritical hydrogen stream.

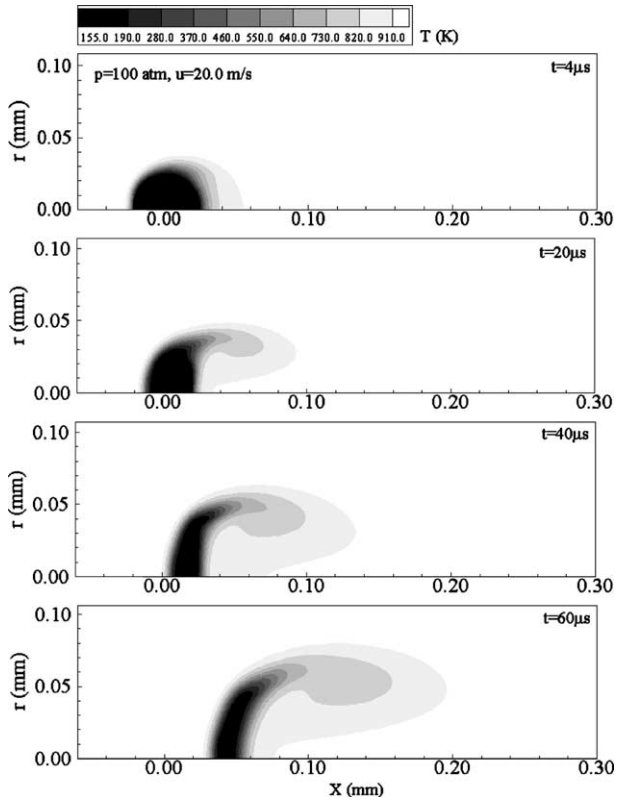

Fig. 11. Temporal evolution of temperature field; liquid oxygen droplet vaporization in supercritical hydrogen stream.

7. Concluding remarks

A unified treatment of general fluid thermodynamics has been developed to treat fluid flows over the entire range of their thermodynamic states, from compressed liquids to dilute gases. The resultant routine is incorporated into a preconditioning scheme, rendering an algorithm valid for all speeds. All of the thermodynamic and numerical properties (such as eigenvalues and Jacobian matrices) are derived directly from fundamental thermodynamic theories, rather than ad hoc approximations for property evaluations. As a consequence, the code is much more robust and efficient than conventional approaches because of its self-consistence and the coherence between the numerics and thermophysics under consideration. The method is general and can accommodate any equation of state for fluid mixtures. As a specific example, a modified Soave–Redlich–Kwong equation of state is employed to derive all of the thermodynamic properties required in the numerical scheme.

As a model validation effort, a series of numerical simulations have been conducted to study supercritical droplet vaporization in both quiescent and convective environments. Results of *n*-heptane droplet vaporization in quiescent nitrogen environments show good agreement with the experimental data on droplet lifetime. The behavior of a liquid oxygen droplet in a supercritical hydrogen stream is also investigated over a broad range of freestream velocity and pressure. The numerical scheme developed in the present study has demonstrated its ability to capture the droplet dynamics and flow evolution. Many salient effects of pressure on supercritical fluid flows are obtained in a computationally robust and efficient manner.

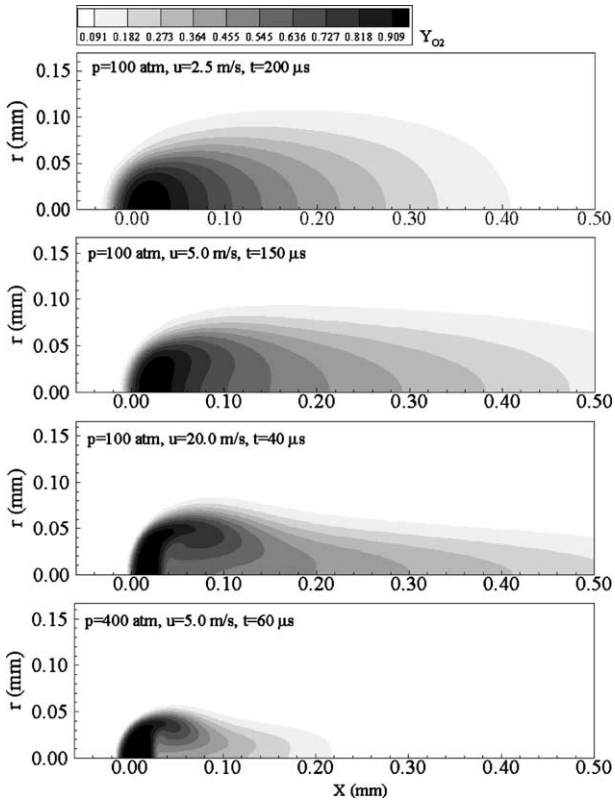

Fig. 12. Distributions of oxygen mass fraction at various ambient conditions; liquid droplet vaporization in supercritical hydrogen stream.

Acknowledgements

This work was sponsored by the Air Force Office of Scientific Research under Grant No. F49620-01-1-0114. The authors gratefully acknowledge the support from Dr. Mitat A. Birkan, contract monitor of the program.

Appendix A

The coefficient matrices in the second-order viscous terms, in Eqs. (5.3) and (5.4), take the following forms:

$$R_{xx} = \begin{bmatrix} 0 & 0 & 0 & 0 & 0 & \cdots & 0 \\ 0 & \frac{4}{3}\mu & 0 & 0 & 0 & \cdots & 0 \\ 0 & 0 & \mu & 0 & 0 & \cdots & 0 \\ 0 & \frac{4}{3}\mu u & \mu v & k & \rho(\bar{h}_1 D_{1m} - \bar{h}_N D_{Nm}) & \cdots & \rho(\bar{h}_{(N-1)} D_{(N-1)m} - \bar{h}_N D_{Nm}) \\ 0 & 0 & 0 & 0 & \rho D_{1m} & \cdots & 0 \\ \vdots & \vdots & \vdots & \vdots & \vdots & \ddots & \vdots \\ 0 & 0 & 0 & 0 & 0 & \cdots & \rho D_{(N-1)m} \end{bmatrix}, \tag{A.1}$$

$$R_{xy} = \begin{bmatrix} 0 & 0 & 0 & 0 & 0 & \cdots & 0 \\ 0 & 0 & -\frac{2}{3}\mu & 0 & 0 & \cdots & 0 \\ 0 & \mu & 0 & 0 & 0 & \cdots & 0 \\ 0 & \mu v & -\frac{2}{3}\mu u & 0 & 0 & \cdots & 0 \\ 0 & 0 & 0 & 0 & 0 & \cdots & 0 \\ \vdots & \vdots & \vdots & \vdots & \vdots & \ddots & \vdots \\ 0 & 0 & 0 & 0 & 0 & \cdots & 0 \end{bmatrix}, \tag{A.2}$$

$$R_{yx} = \begin{bmatrix} 0 & 0 & 0 & 0 & 0 & \cdots & 0 \\ 0 & 0 & \mu & 0 & 0 & \cdots & 0 \\ 0 & -\frac{2}{3}\mu & 0 & 0 & 0 & \cdots & 0 \\ 0 & -\frac{2}{3}\mu v & \mu u & 0 & 0 & \cdots & 0 \\ 0 & 0 & 0 & 0 & 0 & \cdots & 0 \\ \vdots & \vdots & \vdots & \vdots & \vdots & \ddots & \vdots \\ 0 & 0 & 0 & 0 & 0 & \cdots & 0 \end{bmatrix}, \tag{A.3}$$

$$R_{yy} = \begin{bmatrix} 0 & 0 & 0 & 0 & 0 & \cdots & 0 \\ 0 & \mu & 0 & 0 & 0 & \cdots & 0 \\ 0 & 0 & \frac{4}{3}\mu & 0 & 0 & \cdots & 0 \\ 0 & \mu u & \frac{4}{3}\mu v & k & \rho(\bar{h}_1 D_{1m} - \bar{h}_N D_{Nm}) & \cdots & \rho(\bar{h}_{(N-1)} D_{(N-1)m} - \bar{h}_N D_{Nm}) \\ 0 & 0 & 0 & 0 & \rho D_{1m} & \cdots & 0 \\ \vdots & \vdots & \vdots & \vdots & \vdots & \ddots & \vdots \\ 0 & 0 & 0 & 0 & 0 & \cdots & \rho D_{(N-1)m} \end{bmatrix}. \tag{A.4}$$

Appendix B

The numerical Jacobian matrices, T, A, and B, are derived as:

$$T = \begin{bmatrix} -\frac{A_p}{A_\rho} & 0 & 0 & \frac{1}{A_\rho} & -\frac{A_{Y_1}}{A_\rho} & \cdots & -\frac{A_{Y_{N-1}}}{A_\rho} \\ -u\frac{A_p}{A_\rho} & \rho & 0 & \frac{u}{A_\rho} & -u\frac{A_{Y_1}}{A_\rho} & \cdots & -u\frac{A_{Y_{N-1}}}{A_\rho} \\ -v\frac{A_p}{A_\rho} & 0 & \rho & \frac{v}{A_\rho} & -v\frac{A_{Y_1}}{A_\rho} & \cdots & -v\frac{A_{Y_{N-1}}}{A_\rho} \\ \begin{bmatrix} -h_t\frac{A_p}{A_\rho} \\ -1 \end{bmatrix} & \rho u & \rho v & \begin{bmatrix} \rho + \\ \frac{h_t}{A_\rho} \end{bmatrix} & -h_t\frac{A_{Y_1}}{A_\rho} & \cdots & -h_t\frac{A_{Y_{N-1}}}{A_\rho} \\ -Y_1\frac{A_p}{A_\rho} & 0 & 0 & \frac{Y_1}{A_\rho} & \begin{bmatrix} -Y_1\frac{A_{Y_1}}{A_\rho} \\ +\rho \end{bmatrix} & \cdots & -Y_1\frac{A_{Y_{N-1}}}{A_\rho} \\ \vdots & \vdots & \vdots & \vdots & \vdots & \ddots & \vdots \\ -Y_{N-1}\frac{A_p}{A_\rho} & 0 & 0 & \frac{Y_{N-1}}{A_\rho} & -Y_{N-1}\frac{A_{Y_1}}{A_\rho} & \cdots & \begin{bmatrix} -Y_{N-1}\frac{A_{Y_{N-1}}}{A_\rho} \\ +\rho \end{bmatrix} \end{bmatrix}, \tag{B.1}$$

$$A=\begin{bmatrix} -u\frac{A_p}{A_\rho} & \rho & 0 & \frac{u}{A_\rho} & -u\frac{A_{Y_1}}{A_\rho} & \cdots & -u\frac{A_{Y_{N-1}}}{A_\rho} \\ -u^2\frac{A_p}{A_\rho}+1 & 2\rho u & 0 & \frac{u^2}{A_\rho} & -u^2\frac{A_{Y_1}}{A_\rho} & \cdots & -u^2\frac{A_{Y_{N-1}}}{A_\rho} \\ -uv\frac{A_p}{A_\rho} & \rho v & \rho u & \frac{uv}{A_\rho} & -uv\frac{A_{Y_1}}{A_\rho} & \cdots & -uv\frac{A_{Y_{N-1}}}{A_\rho} \\ -uh_t\frac{A_p}{A_\rho} & \begin{bmatrix}\rho u^2\\ +\rho h_t\end{bmatrix} & \rho uv & \begin{bmatrix}\rho u+\\ \frac{uh_t}{A_\rho}\end{bmatrix} & -uh_t\frac{A_{Y_1}}{A_\rho} & \cdots & -uh_t\frac{A_{Y_{N-1}}}{A_\rho} \\ -uY_1\frac{A_p}{A_\rho} & \rho Y_1 & 0 & \frac{uY_1}{A_\rho} & \begin{bmatrix}-uY_1\frac{A_{Y_1}}{A_\rho}\\ +\rho u\end{bmatrix} & \cdots & -uY_1\frac{A_{Y_{N-1}}}{A_\rho} \\ \vdots & \vdots & \vdots & \vdots & \vdots & \ddots & \vdots \\ -uY_{N-1}\frac{A_p}{A_\rho} & \rho Y_{N-1} & 0 & \frac{uY_{N-1}}{A_\rho} & -uY_{N-1}\frac{A_{Y_1}}{A_\rho} & \cdots & \begin{bmatrix}-uY_{N-1}\frac{A_{Y_{N-1}}}{A_\rho}\\ +\rho u\end{bmatrix} \end{bmatrix}, \tag{B.2}$$

$$B=\begin{bmatrix} -v\frac{A_p}{A_\rho} & 0 & \rho & \frac{v}{A_\rho} & -v\frac{A_{Y_1}}{A_\rho} & \cdots & -v\frac{A_{Y_{N-1}}}{A_\rho} \\ -uv\frac{A_p}{A_\rho} & \rho v & \rho u & \frac{uv}{A_\rho} & -uv\frac{A_{Y_1}}{A_\rho} & \cdots & -uv\frac{A_{Y_{N-1}}}{A_\rho} \\ -v^2\frac{A_p}{A_\rho}+1 & 0 & 2\rho v & \frac{v^2}{A_\rho} & -v^2\frac{A_{Y_1}}{A_\rho} & \cdots & -v^2\frac{A_{Y_{N-1}}}{A_\rho} \\ -vh_t\frac{A_p}{A_\rho} & \rho uv & \begin{bmatrix}\rho v^2\\ +\rho h_t\end{bmatrix} & \begin{bmatrix}\rho v+\\ \frac{vh_t}{A_\rho}\end{bmatrix} & -vh_t\frac{A_{Y_1}}{A_\rho} & \cdots & -vh_t\frac{A_{Y_{N-1}}}{A_\rho} \\ -vY_1\frac{A_p}{A_\rho} & 0 & \rho Y_1 & \frac{vY_1}{A_\rho} & \begin{bmatrix}-vY_1\frac{A_{Y_1}}{A_\rho}\\ +\rho v\end{bmatrix} & \cdots & -vY_1\frac{A_{Y_{N-1}}}{A_\rho} \\ \vdots & \vdots & \vdots & \vdots & \vdots & \ddots & \vdots \\ -vY_{N-1}\frac{A_p}{A_\rho} & 0 & \rho Y_{N-1} & \frac{vY_{N-1}}{A_\rho} & -vY_{N-1}\frac{A_{Y_1}}{A_\rho} & \cdots & \begin{bmatrix}-vY_{N-1}\frac{A_{Y_{N-1}}}{A_\rho}\\ +\rho v\end{bmatrix} \end{bmatrix}. \tag{B.3}$$

The numerical Jacobian matrix, $\hat{R}_{xx}$, is derived as

$$\hat{R}_{xx}=R_{xx}\frac{\partial Q_v}{\partial(\hat{Q}/y^\delta)}=R_{xx}\cdot R, \tag{B.4}$$

where R is defined as

$$R=\begin{bmatrix} 1 & 0 & 0 & 0 & 0 & \cdots & 0 \\ 0 & 1 & 0 & 0 & 0 & \cdots & 0 \\ 0 & 0 & 1 & 0 & 0 & \cdots & 0 \\ -\frac{B_p}{B_T} & 0 & 0 & \frac{1}{B_T} & -\frac{B_{Y_1}}{B_T} & \cdots & -\frac{B_{Y_{N-1}}}{B_T} \\ 0 & 0 & 0 & 0 & 1 & \cdots & 0 \\ \vdots & \vdots & \vdots & \vdots & \vdots & \ddots & \vdots \\ 0 & 0 & 0 & 0 & 0 & \cdots & 1 \end{bmatrix}. \tag{B.5}$$

The numerical Jacobian matrix, D, is presented here only with terms related to axisymmetric geometry. Those terms related to chemical reactions can be found in [8]

$$D=\frac{\delta}{y^\delta}\left(D_1-\frac{2}{3}\frac{\partial D_2}{\partial x}-\frac{2}{3}\frac{\partial D_3}{\partial y}+\frac{2}{3}\mu\frac{\partial D_4}{\partial x}\right), \tag{B.6}$$

where

$$D_1 = \begin{bmatrix} 0 & 0 & 0 & 0 & 0 & \cdots & 0 \\ 0 & 0 & 0 & 0 & 0 & \cdots & 0 \\ 1 & 0 & \left[-\frac{4}{3}\frac{\mu}{y} - \frac{2}{3}\frac{\partial \mu}{\partial y}\right] & 0 & 0 & \cdots & 0 \\ 0 & 0 & 0 & 0 & 0 & \cdots & 0 \\ 0 & 0 & 0 & 0 & 0 & \cdots & 0 \\ \vdots & \vdots & \vdots & \vdots & \vdots & \ddots & \vdots \\ 0 & 0 & 0 & 0 & 0 & \cdots & 0 \end{bmatrix}, \tag{B.7}$$

$$D_2 = \begin{bmatrix} 0 & 0 & 0 & 0 & 0 & \cdots & 0 \\ 0 & 0 & \mu & 0 & 0 & \cdots & 0 \\ 0 & 0 & 0 & 0 & 0 & \cdots & 0 \\ 0 & \mu v & \mu u & 0 & 0 & \cdots & 0 \\ 0 & 0 & 0 & 0 & 0 & \cdots & 0 \\ \vdots & \vdots & \vdots & \vdots & \vdots & \ddots & \vdots \\ 0 & 0 & 0 & 0 & 0 & \cdots & 0 \end{bmatrix}, \tag{B.8}$$

$$D_3 = \begin{bmatrix} 0 & 0 & 0 & 0 & 0 & \cdots & 0 \\ 0 & 0 & 0 & 0 & 0 & \cdots & 0 \\ 0 & 0 & 0 & 0 & 0 & \cdots & 0 \\ 0 & 0 & 2\mu v & 0 & 0 & \cdots & 0 \\ 0 & 0 & 0 & 0 & 0 & \cdots & 0 \\ \vdots & \vdots & \vdots & \vdots & \vdots & \ddots & \vdots \\ 0 & 0 & 0 & 0 & 0 & \cdots & 0 \end{bmatrix}, \tag{B.9}$$

$$D_4 = \begin{bmatrix} 0 & 0 & 0 & 0 & 0 & \cdots & 0 \\ 0 & 0 & 0 & 0 & 0 & \cdots & 0 \\ 0 & 1 & 0 & 0 & 0 & \cdots & 0 \\ 0 & 0 & 0 & 0 & 0 & \cdots & 0 \\ 0 & 0 & 0 & 0 & 0 & \cdots & 0 \\ \vdots & \vdots & \vdots & \vdots & \vdots & \ddots & \vdots \\ 0 & 0 & 0 & 0 & 0 & \cdots & 0 \end{bmatrix}. \tag{B.10}$$

Appendix C

The two parameters, $a\alpha$ and $\alpha_{ij}a_{ij}$, in the Soave–Redlich–Kwong (SRK) equation of state, are functions of temperature. Their derivatives with respect to temperature can be expressed in the following forms:

$$\frac{\partial a\alpha}{\partial T} = \sum_{i=1}^{N}\sum_{j=1}^{N} x_i x_j \sqrt{a_i a_j}\frac{\partial \sqrt{\alpha_i \alpha_j}}{\partial T}, \tag{C.1a}$$

where

$$\frac{\partial\sqrt{\alpha_i\alpha_j}}{\partial T}=\frac{1}{2}\left(\frac{\alpha_i}{\alpha_j}\right)^{1/2}\frac{\partial\alpha_j}{\partial T}+\frac{1}{2}\left(\frac{\alpha_j}{\alpha_i}\right)^{1/2}\frac{\partial\alpha_i}{\partial T}, \tag{C.1b}$$

$$\frac{\partial\alpha_i}{\partial T}=-\frac{S_i}{\sqrt{TT_{c,i}}}\left[1+S_i\left(1-\sqrt{\frac{T}{T_{c,i}}}\right)\right], \tag{C.1c}$$

$$\frac{\partial a_{ij}\alpha_{ij}}{\partial T}=\sqrt{a_ia_j}\frac{\partial\sqrt{\alpha_i\alpha_j}}{\partial T}, \tag{C.2}$$

$$\frac{\partial^2 a\alpha}{\partial T^2}=\sum_{i=1}^{N}\sum_{j=1}^{N}x_ix_j\sqrt{a_ia_j}\frac{\partial^2\sqrt{\alpha_i\alpha_j}}{\partial T^2}, \tag{C.3a}$$

where

$$\frac{\partial^2\sqrt{\alpha_i\alpha_j}}{\partial T^2}=\frac{1}{2}\left(\frac{1}{\alpha_i\alpha_j}\right)^{1/2}\frac{\partial\alpha_i}{\partial T}\frac{\partial\alpha_j}{\partial T}-\frac{1}{4}\left(\frac{\alpha_i}{\alpha_j^3}\right)^{1/2}\left(\frac{\partial\alpha_j}{\partial T}\right)^2-\frac{1}{4}\left(\frac{\alpha_j}{\alpha_i^3}\right)^{1/2}\left(\frac{\partial\alpha_i}{\partial T}\right)^2+\frac{1}{2}\left(\frac{\alpha_i}{\alpha_j}\right)^{1/2}\frac{\partial^2\alpha_j}{\partial T^2}+\frac{1}{2}\left(\frac{\alpha_j}{\alpha_i}\right)^{1/2}\frac{\partial^2\alpha_i}{\partial T^2}, \tag{C.3b}$$

$$\frac{\partial^2\alpha_i}{\partial T^2}=\frac{1}{2}\frac{S_i^2}{TT_{c,i}}+\frac{1}{2}\frac{S_i}{\sqrt{T^3T_{c,i}}}\left[1+S_i\left(1-\sqrt{\frac{T}{T_{c,i}}}\right)\right]. \tag{C.3c}$$

The temperature derivatives of the variable, α_{H_2}, are expressed as

$$\frac{\partial\alpha_{H_2}}{\partial T}=-\alpha_{H_2}\left[0.30228\frac{1}{T_{c,i}}\right], \tag{C.4}$$

$$\frac{\partial^2\alpha_{H_2}}{\partial T^2}=\alpha_{H_2}\left[0.30228\frac{1}{T_{c,i}}\right]^2. \tag{C.5}$$

References

[1] V. Yang, Proc. Combust. Inst. 28 (2002) 925.
[2] G.C. Hsiao, Supercritical droplet vaporization and combustion in quiescent and forced-convective environments, Ph.D. thesis, The Pennsylvania State University, University Park, PA, 1995.
[3] P. Lafon, Modélisation et Simulation Numérique de l'Evaporation et de la Combustion de Gouttes à Haute Pression, Ph.D. Thesis, L'Université d'Orléans, France, 1995.
[4] G.C. Hsiao, V. Yang, AIAA Paper 95-0383, 1995.
[5] J.C. Oefelein, V. Yang, Prog. Aeronaut. Astronaut. 171 (1996) 263.
[6] J.C. Oefelein, Simulation and analysis of turbulent multiphase combustion processes at high pressures, Ph.D. Thesis, The Pennsylvania State University, University Park, PA, 1997.
[7] J.C. Oefelein, V. Yang, J. Prop. Power 14 (1998) 843.

[8] J.S. Shuen, K.H. Chen, Y.H. Choi, J. Comput. Phys. 106 (1993) 306.
[9] S.Y. Hsieh, V. Yang, Int. J. Comput. Fluid Dyn. 8 (1997).
[10] H.B. Callen, Thermodynamics and an Introduction to Thermostatistics, Second ed., Wiley, New York, 1985.
[11] M.S. Graboski, T.E. Daubert, Ind. Eng. Chem. Proc. Design Dev. 17 (1978) 448.
[12] M.S. Graboski, T.E. Daubert, Ind. Eng. Chem. Proc. Design Dev. 18 (1979) 300.
[13] R.T. Jacobsen, R.B. Stewart, J. Phys. Chem. Ref. Data 2 (1973) 757.
[14] R.C. Swanson, E. Turkel, J. Comput. Phys. 101 (1992) 292.
[15] P. Jorgenson, E. Turkel, J. Comput. Phys. 107 (1993) 297.
[16] G.E. Schneider, M. Zedan, Numer. Heat Transfer 4 (1981) 1.
[17] Y.H. Choi, C.L. Merkle, J. Comput. Phys. 105 (1993) 207.
[18] P.E.O. Buelow, S. Venkateswaran, C.L. Merkle, AIAA J. 32 (1994) 2401.
[19] J.F. Ely, H.J.M. Hanley, Ind. Eng. Chem. Fundamentals 20 (1981) 323.
[20] J.F. Ely, H.J.M. Hanley, Ind. Eng. Chem. Fundamentals 22 (1983) 90.
[21] S. Takshashi, J. Chem. Engr. (Japan) 7 (1974) 417.
[22] H. Nomura, Y. Ujiie, H.J. Rath, J. Sato, M. Kono, Proc. Combust. Inst. 26 (1996) 1267.
[23] C. Morin, Studies on the influences of pressure and temperature on the vaporization of hydrocarbon droplets, Ph.D. Thesis, Centre National de Recherche Scientifique, Orléans, France, 2000.
[24] B. Vielli, C. Chauveau, X. Chesnau, Proc. Combust. Inst. 26 (1996) 1259.
[25] S. Venkateswaran, C.L. Merkle, AIAA Paper 95-0078, 1995.